# 1

# Mechanisms of Deformation and Failure of Concrete



## 1.1. Concrete: a material that is both widespread and misunderstood

Concrete, the most widely used manufactured material in the world (1 $m^3$ per year and per inhabitant of the planet), is at the heart of the construction of terrestrial infrastructures. Whether it be residential buildings, industrial buildings, energy-producing works, transport infrastructure, etc., concrete, combined with metal to build reinforced concrete structures or prestressed concrete, is present everywhere.

The Romans knew how to make concrete. They discovered that to make a hydraulic binder that would set under water, it was necessary to mix the waste from the manufacture of tiles and bricks or volcanic ash (coming in particular from Pozzuoli, in the bay of Naples, which gave its name to pozzolana, a volcanic rock) with lime. This knowledge, for example, made it possible for them to build harbors protected by concrete piers that set under water, unlike lime. Their knowledge was then lost in the Middle Ages. It was the perfecting and development of the production of modern artificial cements, in particular by Louis Vicat (1817), which allowed the development of current concrete construction. Reinforced concrete boats (1848) by Joseph-Louis Lambot were followed by the creation of entrepreneurs who developed reinforced concrete "systems": François Coignet (1814–1888), who perfected concrete blocks; Joseph Monier, whose patents of 1877 and 1878 were exploited in Germany; François Hennebique (1842–1921), whose company built more than 7,000 structures, most of which still exist; Armand Considere (1841–1914), who invented confined concrete (1901), and many others. In 1906, this first phase ended with the publication of the *Instructions relatives à l'emploi du béton armé*, the first real French regulation for the calculation of reinforced concrete structures, which would lead to the construction of the audacious tower by the architect Auguste Perret in Grenoble in 1924 (see Figure 1.2).

a) b)

**Figure 1.1.** *a) The first cast cement bridge (Louis Vicat, Grenoble, 1853); b) the Glacières Viaduct (France, 1988), truss structure in prestressed concrete (source: P. Paultre and J. Mazars). For a color version of this figure, see www.iste.co.uk/mazars/damage.zip*

a) b)

**Figure 1.2.** *a) The first reinforced concrete tower (Perret Tower, Grenoble, 1924); b) Architectural audacity of the dancing house (Prague, 1996) (source: P. Paultre and J. Mazars). For a color version of this figure, see www.iste.co.uk/mazars/damage.zip*

However, it was the invention of prestressed concrete by Eugène Freyssinet (1879–1962) that opened up new horizons for concrete material. Prestressing consists of keeping the concrete in compression under load by applying a prior stress (prestress) by

means of external jacks or cables under tension installed within the structure itself. It makes it possible to produce original concrete structures in terms of their shape, lightness and mechanical audacity (see Figure 1.1).

Admittedly, concrete exists in several categories, ranging from the most rustic – concrete used for self-construction – to the most elaborate – very high performance concretes resulting from mixtures of ingredients and specific manufacturing processes. However, in any case, getting it to hold up well under load and over time is a tricky problem to address. Figure 1.3 shows all the complexity, from the moment of pouring until the long term: a varied number of phenomena related to the maturation of the concrete, the application of the loads or the aging intervene.

At the heart of these problems, there is the progressive degradation of the material of a thermohydromechanical nature or under the effects of time. The purpose of this book is to propose modeling tools based in particular on fundamentals in solid-state physics and damage mechanics, making it possible to help engineers solve a number of questions mentioned in Figure 1.3.

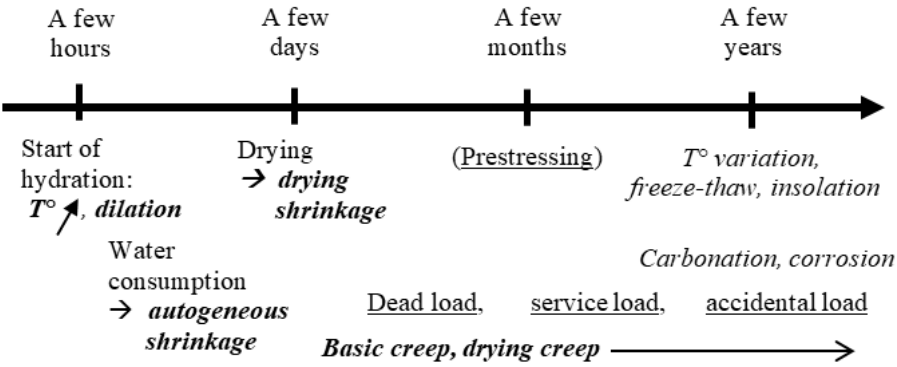


**Figure 1.3.** *Phenomena acting on concrete during the life of a structure; in bold italics, the physicochemical effects; underlined, the loads applied; in italics, climate and environmental actions (Lavinia et al. 2010)*

This summary presentation could advantageously be supplemented by the following documents: Pliskin (1995), Merceron-Vicat (1999) and Association Freyssinet (2004).

## 1.2. Composition and behavior of concrete at an early age

Concrete results from the mixture of the following main ingredients:

– cement, which is a hydraulic binder (hardening under the action of water) obtained by firing at 1,450°C a mixture of limestone and clay (clinker) that is finely ground with additions, giving it specific characteristics;

– aggregates, which include sand (grains up to 5 mm) and gravel (grains from 5 to 25 mm for common concretes);

– water, any additives used to control or promote certain properties (delay or acceleration of setting, plasticity of fresh concrete, etc.), as well as air occluded during placement in molds.

The proportions for common concretes are given in Table 1.1. The whole of this is introduced into a mixer adapted to the volume to be processed to constitute a mixture that is as homogeneous as possible.

In addition, for certain applications, it is possible, by playing on the quality of the different ingredients, to obtain special concretes: light concretes or heavy concretes by the use of suitable aggregates (expanded clay, barite or magnetite aggregates), high-performance concrete (additions of ultrafine silica fumes), fiber-reinforced concrete (additions of metallic or organic fibers), etc.

| | **Water** | **Air** | **Cement** | **Aggregates** |
|---|---|---|---|---|
| **Volume (in %)** | 14–22 | 1–6 | 7–14 | 60–78 |
| **Weight (in %)** | 5–9 | | 9–18 | 65–85 |

**Table 1.1.** *Order of magnitude of the proportions of the constituents for common concrete (according to CimBéton (2013))*

Figure 1.4 shows, at three different scales, the main aspects of the microstructure of hardened concrete:

– decimetric scale (that of the volume element, in the mechanical sense of the term), showing the different sizes of aggregates and the cementitious matrix;

– centimeter scale, showing the cracking of the matrix between grains, which may result from effects linked to maturation or from premature mechanical loading;

– micrometric scale, for which the microstructure of the hydrated cement paste appears.

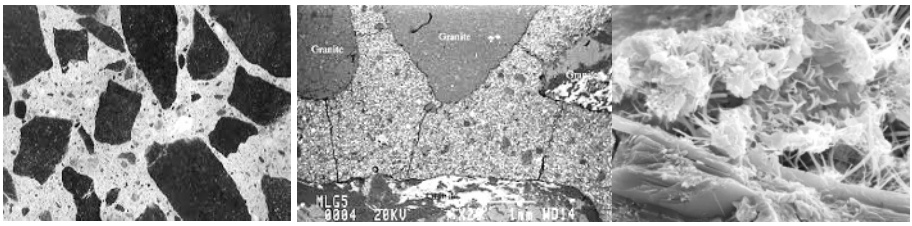


a) b) c)

**Figure 1.4.** *Three levels of concrete microstructure: a) volume element (in the mechanical sense), b) grain scale and c) microstructure of the hydrated cement, which is a tangle of C-S-H and ettringite needles (from Aftes (2012) and CimBéton (2013))*

### 1.2.1. *Concrete curing*

The major elements contained in the cement that intervene during hydration are the silicates. In contact with water, the tricalcium silicates ($Ca_3SiO_5$) and the dicalcium silicates ($Ca_2SiO_4$) contained in the cement dissolve in the form of ions, which interact with each other and form hydrated calcium silicates ($(CaO)x(SiO_4)y(H_2O)z$), C-S-H in simplified form, and portlandite ($Ca(OH)_2$). These reactions are exothermic.

C-S-H are non-crystalline compounds. They have the characteristics of a gel and have a variable composition; their average composition is close to $(CaO)_{1.7}(SiO_4)(H_2O)_4$. The entanglement of the C-S-H gel gives cement its solidity: it develops on the surface of the non-hydrated cement grains and progressively fills in the capillary pores between the grains (see Figure 1.5).

After a few hours, the layer of hydrates that coats the cement grains becomes thick enough to slow down the diffusion of ions and water toward the anhydrous components of the system. Hydration slows down more and more but can continue for months, or even years.

However, tricalcium aluminate is also present, which is the cement compound that is the most reactive with water. This is because the hydration of aluminates is so rapid that cement manufacturers add gypsum to the clinker to control their reactions. Aluminates react with gypsum sulfate to form ettringite TSA (hydrated calcium trisulfoaluminate). This reaction is highly exothermic. A layer of hydrates surrounds the aluminates, which then form a protective layer around the grain of cement. When the gypsum is exhausted, the sulfate concentration of the solution drops; the ettringite then becomes unstable and dissolves to form hydrated calcium

monosulfate. After a few weeks, in general, the ettringite is completely transformed into monosulfoaluminate (called AFm).

As we have just seen, the hydration of Portland cement involves the reaction of the various mineral phases that compose it. As cement is mainly composed of tricalcium silicates, it is the hydration of the C3S that controls the overall kinematics of hydration. However, there is a synergy between the different reactions. Figure 1.5 indicates the main phases of hydration, which, from the start of setting, lead to the formation of a solid that undergoes heating then cooling at the same time as it hardens (improvement of mechanical properties).

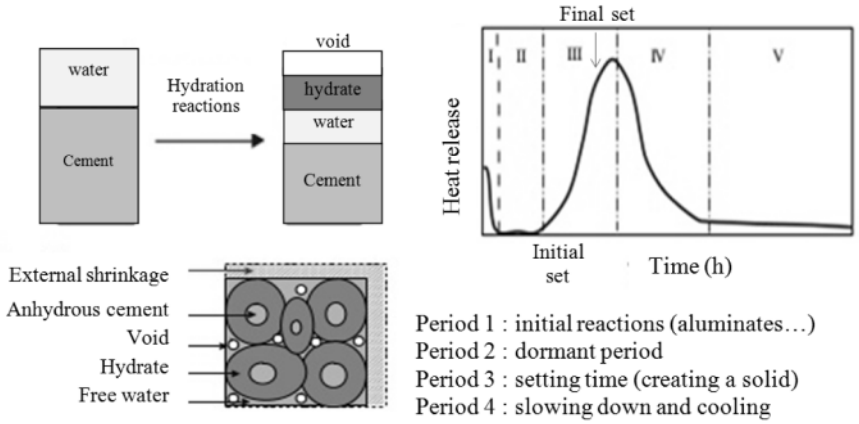


**Figure 1.5.** *Cement hydration mechanisms showing the exothermicity of the reaction and the autogenous shrinkage it induces*

However, concrete includes, in addition to water and cement, aggregates: sand and gravel. The hydration of the cement occurs in this highly heterogeneous medium, which leads to thermomechanical reactions during the chemical process. Indeed, aggregates are generally inert materials, but are sensitive to heating and shrinkage of the cementitious matrix. This is how they will play a dual role during the maturation phases:

– guiding the development of hydration products creating a different microstructure near the aggregates (particularly the larger ones), thus enclosing a zone called the "transition zone" likely to create local mechanical weakness;

– constitute hard points during the retraction of the material (see Figure 1.5) showing that the final volume of the hydrated products is lower than the initial volume, in

particular due to the consumption of water during the chemical reaction. The grains oppose this shrinkage, which generates internal stresses within the matrix and risks of damage, as shown in Figure 1.4(b).

On the scale of a structural element, these cumulative dilation-shrinkage phenomena can lead, when these movements are hampered by specific boundary conditions, to cracking (see Figure 1.6).

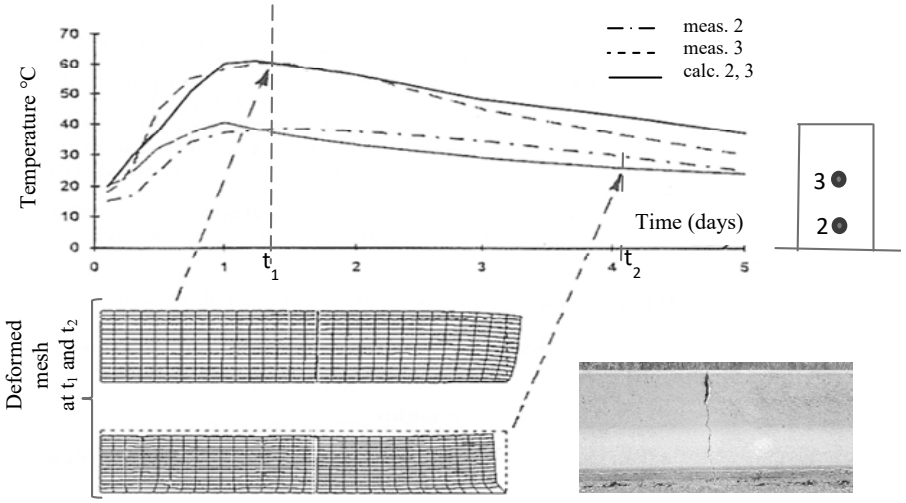


**Figure 1.6.** *Cumulative consequences of dilation-shrinkage effects in a concrete element whose movement is hampered by its adhesion to the supporting soil; the strains are amplified (according to Mazars and Bournazel (1998))*

SUMMARY.– *The hydration of cement, which leads to the maturation of concrete, is accompanied by physicochemical phenomena that generate*:

*– on the barely solid material (beginning of setting), a dilation created by the exotherm of the reaction (see Figure 1.8(a));*

*– on the material at already advanced maturity (end of setting), the accumulation of cooling and shrinkage (autogenous shrinkage created in particular by the reduction in the overall volume of the products entering the hydration reaction (see Figure 1.5)), which cause structural stresses internal to the material likely to cause them at the level of the structural elements according to the hamper to the strain brought by the boundary conditions.*

It is important to note that the development of stresses that apply to a material of viscous nature leads to the generation of relaxation (lowering of the stress at imposed strain) and/or creep (increase of the strain at imposed stress). At an early age, it is generally relaxation that prevails, and its effect is mechanically positive by limiting the risk of damage.

### 1.2.2. *Consequences of curing and phenomena related to the aging of concrete*

The lessons from section 1.2.1 allow us to consider that two zones of importance appear in the microstructuring of common concrete:

– the cementitious matrix-aggregate bond where a less resistant zone is observed due to:

- the specific structuring of hydrates;

- the existence of microvoids from air bubbles or water droplets trapped in particular under the grains during placement in the molds;

- any microcracks resulting from the hard spot effects of the aggregates during the shrinkage of the matrix (see Figure 1.4(b));

– the matrix outside this bond is dotted with capillaries of micrometric dimension, vestiges of those existing in fresh concrete and micropores, linked to the very formation of hydrates, the size of which is of the order of a few tens of Angstroms (see Figure 1.7(a)).

In general, as shown in Figure 1.7(b), the strength of concrete (here, under compression) decreases with the porosity of the material, which will mainly depend on the water/cement (W/C) ratio of the initial mix. The greater the W/C is, the more excess water there is in the concrete after maturing, which increases the porosity accordingly (the capillaries are filled with air or water). This greater porosity has two consequences:

– the material is less compact and less resistant;

– the capillaries are often interconnected (unlike the pores of hydrates), which increases the permeability of the material.

This open porosity promotes the evaporation of water from the capillaries, which generates a retraction of the material: drying shrinkage or desiccation shrinkage, which is added to the autogenous shrinkage due to hydration (see Figure 1.8(b)). In addition, this desiccation acts on the creep behavior (strain under imposed stress) by

generating, in addition to the basic creep linked to maturation, a drying creep which, like the drying shrinkage, acts in the long term (Ollivier et al. 2012).

All of this information leads to a better understanding of Figure 1.3, confirming the different physical phenomena that accompany the maturation of concrete at an early age and the aging of mature concrete. To all this, it is now necessary to add the effects of mechanical loadings; this is what we propose for analysis in section 1.3.

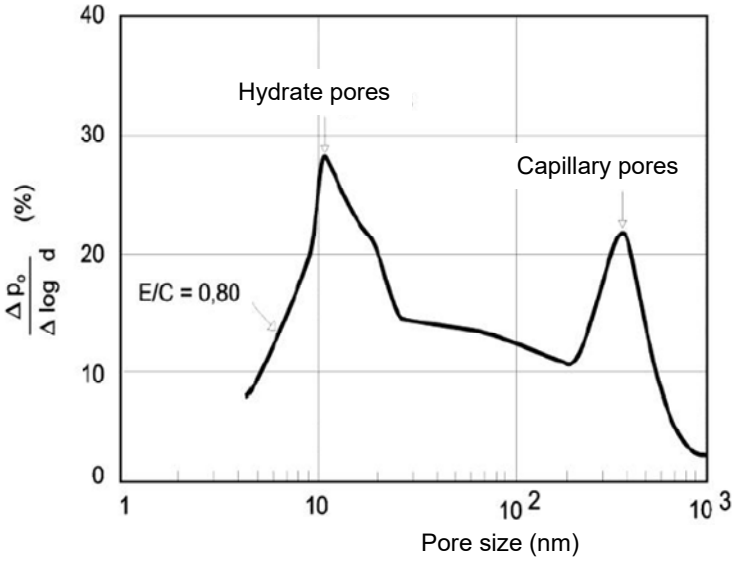


a)

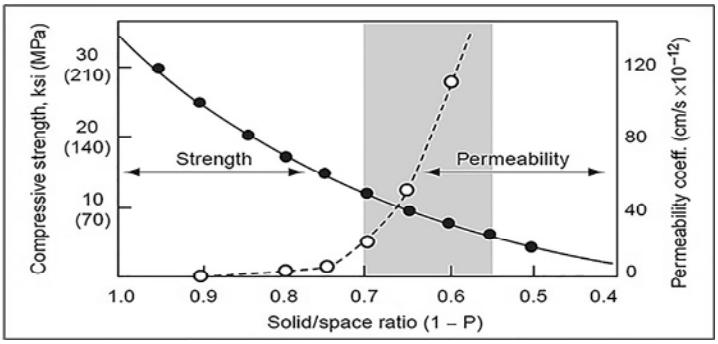


b)

**Figure 1.7.** *Porosity and strength. a) The two categories of pores (Verbeck et al. 1968); b) decrease in the compressive strength and increase in the permeability of concrete with the increase in its porosity P (according to Hilal (2014))*

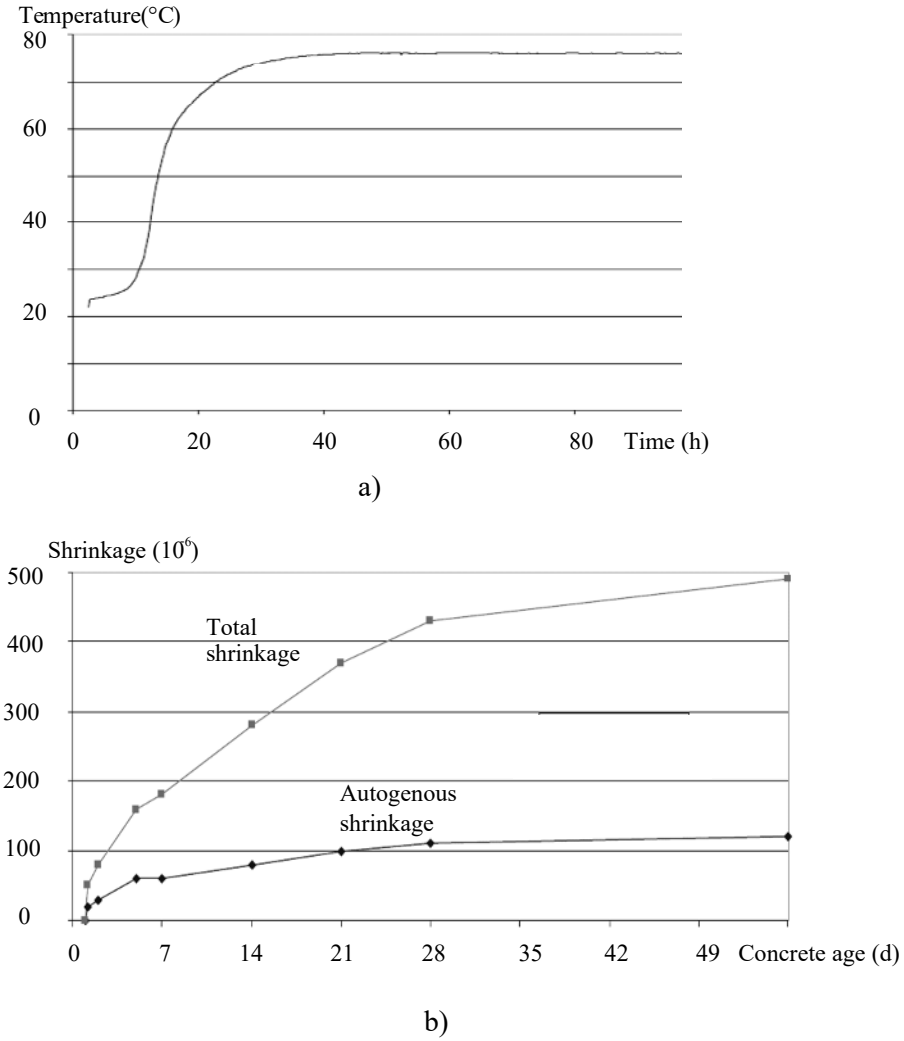


**Figure 1.8.** *Phenomena of early age of C50/60 concrete. a) Temperature rise during hydration measured under adiabatic conditions; b) autogenous and total shrinkage: autogenous + desiccation (according to CEOS (2017))*

## 1.3. Main aspects of the mechanical behavior of concrete

### 1.3.1. *Concrete under uniaxial loading*

#### 1.3.1.1. *Uniaxial compression*

The failure properties of the material under compression are at the center of the characteristics used by the designers of concrete structures who rely on standards and codes to work. First, concretes are designated by their resistance class: for example, C 30/37 corresponds to a characteristic compressive strength of 30 MPa on a cylinder and 37 MPa on a cube. These strengths are characteristic strengths $f_{ck}$ (defined at the fractile 5%) of hardened concrete at 28 days.

Cylinder strength occurs on specimens twice as high as they are wide, at least 110 mm in diameter (in France, cylinders are 160 mm in diameter and 320 mm in height). The cube strength $f_{ck}$ is higher because, due to the interactions between the press platens and the specimen (friction locally generating a lateral pressure), the incidence is felt up to the middle of the cube; the stress state then has a triaxial character, which artificially improves its strength. Having a cylinder of height that is twice the diameter (or more) makes it possible to provide, in the center of the specimen, an area in quasi-uniaxial compression (see Figure 1.9(a)). From this $f_{ck}$ value at the fractile 5%, which means that in a batch of specimens tested, 95% of them have a strength greater than $f_{ck}$, a number of characteristics are deduced according to Eurocode 2 (2004):

– the average value of compressive strength: $f_{cm} = f_{ck} + 8$ MPa;

– the calculation strength: $f_{cd} = f_{ck}/\gamma_c$ ($\gamma_c = 1.2$ for accidental situations, 1.3 for earthquakes, 1.5 for long-term or transient situations);

– the "instantaneous" modulus of elasticity: $E_{cm} = 2{,}200\ (f_{cm}/10)^{0.3}$ MPa;

– the "delayed" modulus (taking creep into account): $E_{c,eff} = E_{cm}(t_0)/(1 + \varphi(t_0))$, $t_0$ age at first loading and $\varphi(t_0)$ creep coefficient (current case, $\varphi(t_0) = 2$);

– the average tensile strength: $f_{ctm} = 0.3(f_{ck})^{2/3}$ MPa, if $f_{ck} < 50$ MPa and $f_{ctm} = 2.12\ \ln(1 + f_{cm}/10)$ MPa if $f_{ck} > 50$ MPa, from which we deduce the characteristic strength $f_{ctk,0.05} = 0.7\ f_{ctm}$ and the calculation strength $f_{ctd} = f_{ctk}/\gamma_c$ ($\gamma_c$ as defined for the compression).

Thus, the designer has an arsenal of values that make it possible to approach a project for new structures within the framework of the corpus of rules established by the Eurocode and its national appendices. Eurocode 2 (2004) also provides relationships for estimating strength to early age, shrinkage, creep, etc.

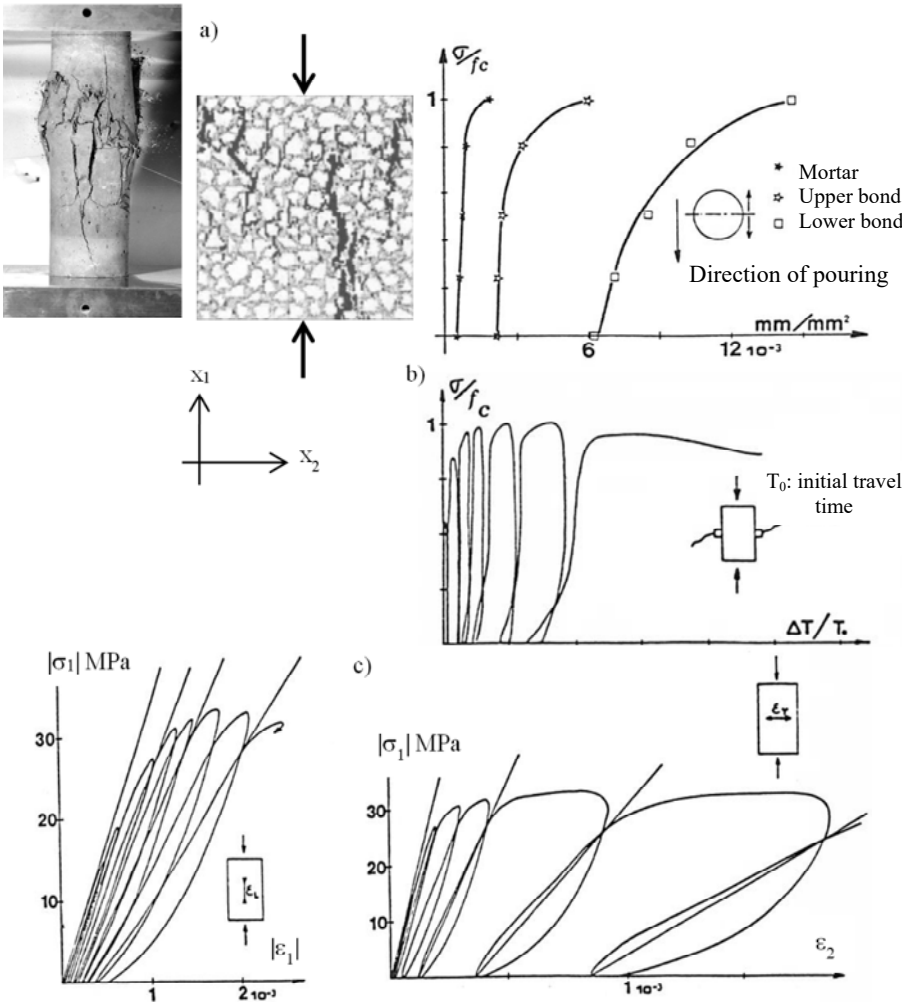


**Figure 1.9.** *Behavior of concrete under compression. a) Experimental cylinder failure and fracture facies on a meso-model; b) progression of microcracks within the mixture and evolution of ultrasonic waves in the transverse direction ($x_2$) of the sample; c) $|\sigma_1|$–$|\varepsilon_1|$ and $|\sigma_1|$–$\varepsilon_2$ curves, with discharges, showing the evolution of stiffness (from Mazars (1984))*

The use of the modeling strategies proposed in this book is outside the corpus of Eurocodes, but when certain test results are not available at the time of calculations, data from previous relationships may be needed. In this case, *it is the average strengths that are to be considered* and not the characteristic strengths that are

values including a certain safety, and whose use would distance the results obtained from the reality that the present models must approach as closely as possible to carry out a relevant structural analysis.

With regard to the uniaxial compression behavior of ordinary hardened concrete, Figure 1.9 provides information on the overall microstructural and mechanical response. Indeed, we note that:

– the failure is obtained by multicracking with the orientation of the cracks being globally parallel to the direction of the load (see Figure 1.9(a));

– the monitoring of microcracking during the test leads to the observation of cracking present before loading, mainly in the lower bond of the largest grains (compared to the direction of pouring) and that it is around the grains that the cracking first progresses, before spreading in the matrix as it approaches failure (see Figure 1.9(b));

– the curve of evolution of the velocity of ultrasonic waves in the direction $X_2$ is characteristic of the opening of cracks, especially approaching the maximum stress and beyond, where a runaway phenomenon appears at the same time as failure (see Figure 1.9(a)).

The global curves $|\sigma_1| - |\varepsilon_1|$ and $|\sigma_1| - \varepsilon_2$ exhibit three stages (see Figure 1.9(c)):

– a quasi-elastic zone, 30–40% $f_c$ ($f_c$ = compressive strength), a period during which the initial microcracking does not progress; the modulus of elasticity E is constant, as is Poisson's ratio $\nu$;

– a nonlinear zone with increasing stress (pre-peak), the cracks progress around the aggregates, and the modulus of elasticity E of the material decreases (see the slopes of the load-unload loops in Figure 1.9(c)), but the Poisson's ratio barely changes;

– a nonlinear zone with decreasing stress (post-peak), the cracks develop more and more in the matrix and open (see evolution of ultrasonic velocities in Figure 1.9(b)), transverse strains $\varepsilon_2$ are amplified and the apparent Poisson's ratio greatly increases: this is the failure (see Figure 1.9(a)).

The load–discharge curves (see Figure 1.9(c)) show, in addition to the evolution of the stiffness, the presence of hysteresis loops, which are characteristic of energy dissipation, mainly due to friction between the lips of cracks that are close. Also present are permanent strains at zero stress; the explanation that can be given is that they are the manifestation of the release of internal stress created during the maturation of the material (see section 1.2). Once these stresses have been released, the microcracked medium does not return to its reference state at zero stress, which generally results in residual strains.

NOTE 1.1.– The determination of the modulus of elasticity and Poisson's ratio is carried out from curves such as those presented in Figure 1.9(c). The details of obtaining them are given in the exercises part of the book (see section 9.1).

### 1.3.1.2. *Uniaxial tension*

Overall, the tensile strength of ordinary concrete is an order of magnitude lower than its compressive strength. For the design engineer, this is still a useful property, but is of less importance than compression.

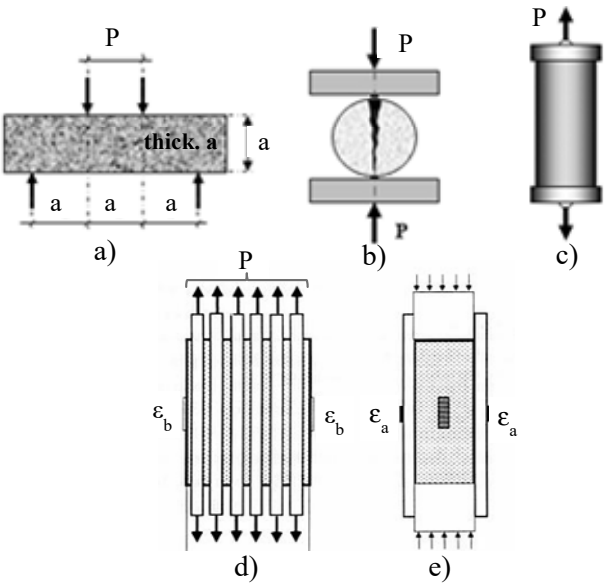


**Figure 1.10.** *Different types of tests for analyzing behavior. a) Tension by bending; b) tension by splitting; c) direct tension; d) and e) direct tension-compression to multicrack and analysis of the unilateral character of cracked concrete*

This is for several reasons:

– apart from a few structures such as dams, concrete is rarely used alone; it is either reinforced (the reinforcements being mainly present to overcome the deficiency of concrete tensile strength) or prestressed (the structure is placed in a state of permanent compression to avoid weaknesses due to tension);

– testing concrete under tension is less easy and therefore less widespread than the compression test. This led the coder, as indicated in section 1.3.1.1, to define the tensile properties according to the results of the compression tests.

This being said, the cracking of structures is totally controlled by the tensile properties and this is throughout the total life of the structure (from an early age to a long time). This has major consequences on the durability of structures and some specific properties, such as sealing for reservoirs and containment structures.

Figure 1.10 shows the variety of tests that are performed to test concrete under tension. From left to right:

– the tension by bending test, easy to perform on a prismatic specimen (in France, dimension a is 100 mm); the concrete cracks on the lower side by failure under tension, we suppose that the behavior is linear until the failure and, for the maximum load, we deduce the tensile stress at failure;

– the tension by splitting test, a compressive load applied on a diameter of the test cylinder, leads to a distribution of tensile stresses perpendicular to the diameter and, as before, assuming that everything happens linearly until failure, the tensile stress at failure is deducted from the maximum load;

– the direct tension test, generally carried out on a cylinder of constant or variable section, to locate the failure, which always appears as a crack perpendicular to the direction of the load;

– the test making it possible to cause multicracking to obtain more information on post-peak behavior. This same test makes it possible to exert, following tension (see Figure 1.10(e)), compression to analyze the unilateral nature of the concrete behavior under alternating loading (restoration of the stiffness with the closing of the cracks).

In the rest of this section, we will only analyze the behavior under direct tension of the last two types of tests, but we will return to the others (tension by bending and splitting) in Chapter 4 in regard to comparing the results of these tests, which must be done with correctness, within the framework of the identification of the parameters of the damage models.

Figure 1.11 gives the essential elements that make it possible to understand the particularities of concrete under direct tension, which will be useful to model its behavior.

Two main phases appear as follows:

– a quasi-linear phase up to the peak (see Figure 1.11(b)), where the material remains quasi-elastic linear;

– a post-peak phase, resulting from the instability created by the formation of a localization of microcracks that coalesce into a main crack, which causes a sudden drop in stress as the strains continue to grow, as well as a significant stiffness loss (see Figure 1.11(b)).

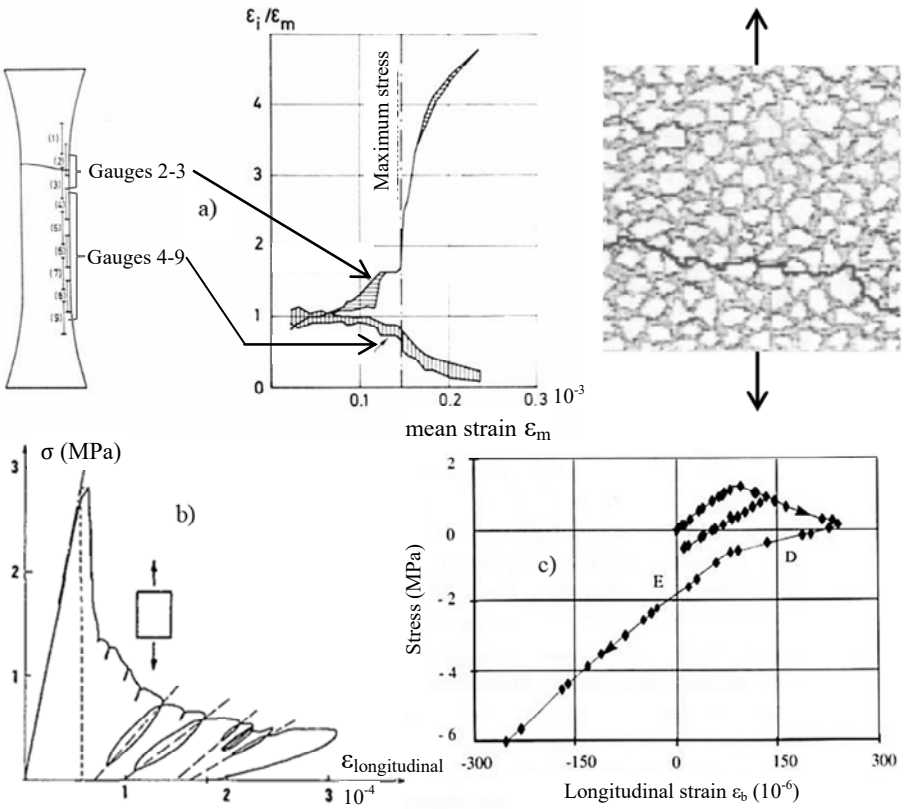


**Figure 1.11.** *Behavior under direct tension. a) Localization of strains and final cracking (according to Heilmann et al. (1969)); b) overall mechanical behavior (according to (Terrien 1980)); c) particularity of the behavior resulting from the test creating a multicracking and allowing alternate loading (according to Mazars et al. (1989))*

The crack is generally intergranular and globally oriented perpendicular to the direction of the force. The measurements made by Heilmann et al. (1969) (see Figure 1.11(a)) provide a better understanding of the localization process because of the measurement of strains by gauges at and around the crack. While the strains of gauges 2 and 3, through which the crack passes, progress compared to the average strain of the specimen $\varepsilon_m$, the strains measured by gauges 1, 4 and 9, which are around this zone, regress. This redistribution of the deformations inside the specimen is characteristic of the appearance of the localization, which is noticeable before the peak. The specimen is no longer in a uniform field (stress and strain) and becomes a structure that the models will have to know how to simulate.

In the so-called multicracking test (see Figures 1.10(d) and 1.10(e)), the tensile force is exerted on the parallelepipedal sample by means of aluminum rods glued to the large sides of this sample. Thus, these rods apply a state of uncontrolled strain on either side of the specimen, which prevents any premature localization. The material here is microconcrete, and at the end of the tensile sequence, multicracking appears (four to five cracks barely visible to the naked eye), indicating that the degradation is widely distributed inside the material; we will discuss diffuse damage here. A second sequence is then carried out by freeing the rods of all forces and applying compression directly to the two extremities of the specimen. The curve (see Figure 1.11(c)) results from a post-processing of the global force-strain curve concerning the assembly ($\varepsilon_1$ measured at the center of the specimen), from which the forces passing through the bars of the assembly must be deducted (these remain elastic throughout the entire test).

From these results, it can be seen that:

– we find the phases of tensile behavior already seen in the direct tension test: quasi-elasticity up to the peak, then beyond that a drop in stiffness and stress, less brutal than in the direct tension test;

– the subsequent compression phase highlights a restoration of the stiffness due to the closure of the cracks created under tension, which leads to almost regaining the initial stiffness and reducing the permanent strains resulting from the tension phase. This phenomenon is called the "unilateral effect" (Mazars et al. 1990); it plays a major role in the behavior of concrete structures under alternating loads, such as earthquakes.

In fact, this test is representative of the tensile effects on concrete in the presence of reinforcement, the role of which is played here by the bonded aluminum bars.

NOTE 1.2.– The compressive and tensile properties for a given concrete are dependent on the loading rate measured in strain rate. We will take up this point in detail in Chapter 6 during the studies on the simulation of rate effects. It is shown that the phenomenon is especially marked under tension for high velocity (the resistance is multiplied by 2, 3, 4, respectively, for $\dot{\varepsilon} = d\varepsilon/dt = 10^{-1}$/s, 1/s, $10^{2}$/s) (below $\dot{\varepsilon} = 10^{-2}$/s, the increase is not significant and may not be taken into account). Under compression, the effects are much less marked (approximately 1.3 for $\dot{\varepsilon} = 1$/s). In Chapter 6, we show how these aspects must be considered to address situations of rapid dynamics and, in particular, of impact on structures.

NOTE 1.3.– Among the different types of concrete exists the so-called high-performance concrete (HPC), which is a highly compact material obtained by the addition of elements allowing for the deflocculation of the cement grains and by extension of the granular mixture toward very thin elements (limestone fillers, silica

fume, etc.), which, in addition to better compactness, makes it possible to limit the quantity of water necessary for implementation. The resulting hardened material has significantly improved properties in strength and durability (drastic reduction in open porosity). Figure 1.12(a) shows an example of the behavior under compression of this type of concrete ($f_c$ = 105 MPa, E = 51 GPa), which shows quasi-elastic behavior up to failure and very brittle behavior beyond that. The same concrete has a tensile strength, measured in the splitting test, of 6.5 MPa.

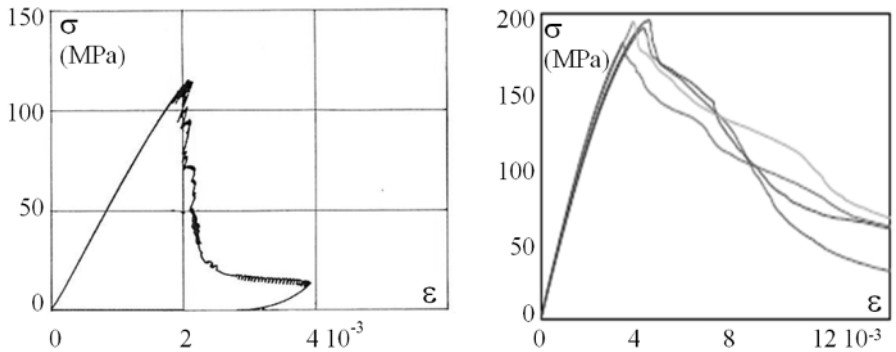


**Figure 1.12.** *Behavior in compression of special kinds of concrete: a) high-performance concrete (HPC); b) ultra-high-performance fiber-reinforced concrete (UHPFRC) (according to Jungwirth and Muttoni (2004)). For a color version of this figure, see www.iste.co.uk/mazars/damage.zip*

Figure 1.12(b) gives an example of another category of concrete: ultra-high-performance fiber reinforced concrete (UHPFRC), whose composition ensures good compactness and includes fibers that are generally, but not exclusively, metallic. Due to a very controlled manufacture, the compressive strengths reach 200 MPa and higher.

The behavior is characterized by:

– a range of elastic strain limited by the strength at extension of the cementitious matrix;

– a post-cracking domain characterized by the tensile strength of the fiber material obtained after the cracking of the matrix.

This leads to a very softened post-peak, which settles on large strains and gives it a kind of ductility.

The models presented in the following chapters focus on so-called “ordinary” kinds of concrete with an average strength of up to 60–70 MPa. Beyond that, we fall

into the category of special kinds of concrete, and it goes without saying that the modeling of these concrete types must be adjusted in relation to those presented in this book.

### 1.3.2. *Concrete under multiaxial loading*

From the analyses made with respect to uniaxial loading, we remember in particular that the directions of cracking are:

– under tension, perpendicular to the direction of the force;

– under compression, parallel to the direction of the force.

The common denominator of these two situations is that the cracks are globally perpendicular to the directions of extensions ($\varepsilon > 0$). This crack opening mode is called "mode I".

Mode I promotes unstable behavior (present under compression beyond the peak and very marked under tension). The presence of a stress in one or two complementary directions changes the response of the material.

The addition of one or two tensile directions will favor the development of mode I in their respective orthogonal direction, which tends to weaken the strength in the initial direction, whether loaded under compression or under tension.

With the addition of compression, the cracking facies obtained are illustrated in Figure 1.13a (Kupfer et al. 1969):

– if the original stress is tension, this compression will add extensions in the direction of the tension, favor mode I and consequently weaken the corresponding strength;

– if the original stress is compression, this new compression will hamper the development of mode I in an orthogonal direction, which creates a kind of confinement in the bicompression plane that is as strong as this stress is intense, and the strength is increased. Figure 1.13(b) shows the effect of this additional compression on the variation in volume of the material.

With the addition of two compressions:

– if the original stress is tension, the observation is the same as that expressed for the addition of one compression, and the strength under tension is weakened;

– if the original stress is compression, depending on the relative intensity of the three compressions, the development of mode I is increasingly hampered, and we

are then in the most favorable cases of strength. We will discuss this particular situation in detail in section 1.3.2.2 by considering two cases: where the extensions remain possible and where they are no longer, for which new modes of cracking in shear (mode II) will develop.

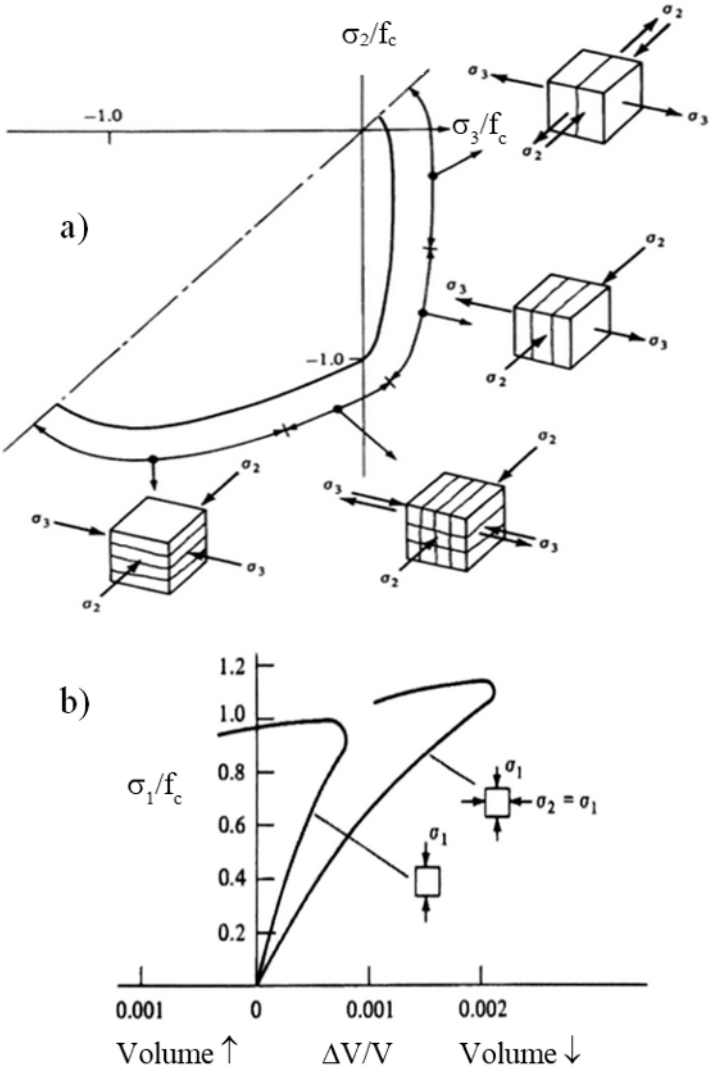


**Figure 1.13.** *Biaxial loading ($\sigma_3 = 0$). a) Facies of degradation under biaxial loading; b) influence of confinement on the volume variation ($\Delta v/v = \varepsilon_1 + \varepsilon_2 + \varepsilon_3$)*

### 1.3.2.1. *Behavior under biaxial loading*

A series of authoritative experimental results on this subject are those of Kupfer and Gerstle (1973). Performed on parallelepipedal specimens (200 × 200 × 50 mm) for three kinds of concrete of different uniaxial compressive strengths ($f_c$ = 19.1 – 32.8 – 59.4 MPa). They show that the shape of the failure surface in the plane $\sigma_3 = 0$ (normalized by the compressive strength $f_c$) is very close, which is major information for establishing a model (see Figure 1.14(a)).

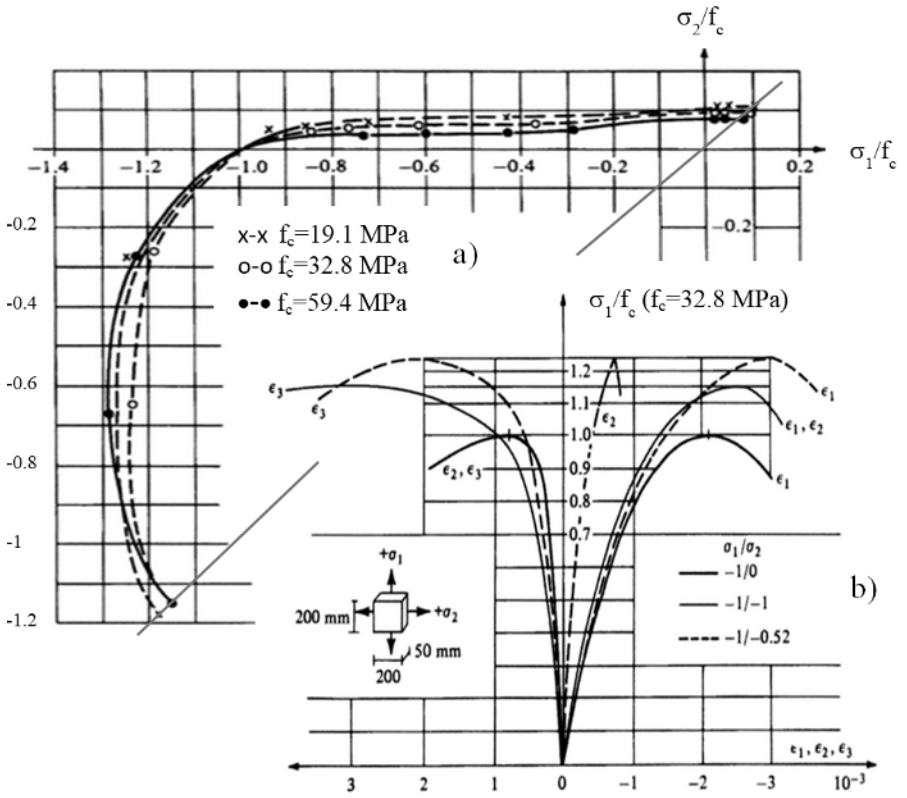


**Figure 1.14.** *Experimental results under biaxial loading (source: Kupfer et al. 1973): a) trace of the failure surface in the plane $\sigma_3 = 0$, for three different kinds of concrete; b) comparison of behavior for concrete $f_c$ = 32.8 MPa and for three ratios $\sigma_1/\sigma_2$ (–1/0, –1/–1, –1/–0.52); we can note the increase in strength with the intensity of confinement. For a color version of this figure, see www.iste.co.uk/mazars/damage.zip*

This failure surface confirms the observations made on the incidence of the addition of orthogonal loading to uniaxial loading in the three sectors:

tension-tension (little difference with the uniaxial strength), tension-compression (weakening tensile strength) and compression-compression (increase in compressive strength due to the confinement created).

On the compression-compression sector, Figure 1.14(b) shows, for concrete $f_c$ = 32.8 MPa, the behavior for three different bicompression ratios (($\sigma_1/\sigma_2$ = −1/0, −1/−1, −1/−0.52).

It can be seen that it is for the ratio $\sigma_1/\sigma_2$ = −1/−0.52 that the strength is the greatest, approximately 1.25 times the uniaxial compressive strength, while it is only 1.15 when $\sigma_1 = \sigma_2$.

It is also noted that the failure processes are of the same nature for bicompression as for uniaxial compression: linearity up to approximately one-third of the strength, progressive nonlinearity with increasing stress up to the peak and then an amplification of the strains of extension ($\varepsilon_3$), which translates the formation and the opening of cracks in mode I in direction 3, which quickly leads to the collapse of the sample in layers parallel to the plane of loading.

#### 1.3.2.2. *Behavior under triaxial loading of compression*

Figure 1.15 shows the two main types of triaxial tests:

– the test using a prism on which the three orthogonal stresses are exerted; this is done by a system of jacks and interface plates, which must allow all the strains during the test, which is not simple; it is said to be "true" triaxial because all of the combinations of compressions are possible on the three axes (see Figure 1.15(a));

– the test in a triaxial cell (see Figure 1.15(b)); inherited from soil mechanics, it is carried out on a cylinder that receives a lateral pressure under the effect of a pressurized fluid (sealed protection is necessary at the interface between the fluid and the specimen) and a vertical stress via an axial jack, which leads to an axisymmetric stress state ($\sigma_1 \neq \sigma_2 = \sigma_3$).

In both cases, the experimental system is complex and expensive. It requires real expertise for its use (the realization of measurements often poses problems). Triaxial cells with high confinement exist in some laboratories around the world and make it possible to carry out tests whose results can be used to simulate impacts on structures (the pressures under impactors are indeed highly triaxial and very intense).

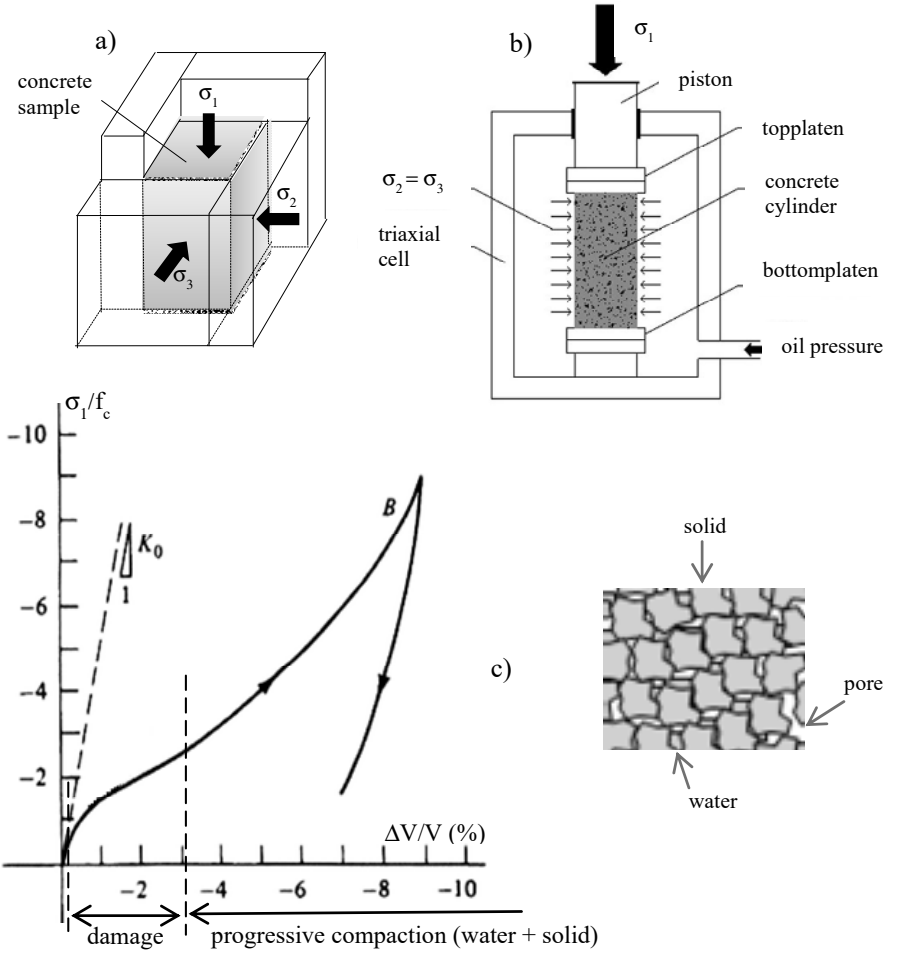


**Figure 1.15.** *Triaxial tests for concrete: a) "true" triaxial ($\sigma_1 \neq \sigma_2 \neq \sigma_3$); b) confinement cell ($\sigma_1 \neq \sigma_2 = \sigma_3$); c) response of a concrete specimen to a hydrostatic load ($\sigma_1 = \sigma_2 = \sigma_3$) showing, after the collapse of the microporous structure, the compaction of water and solid (according to Rouquand et al. (2007)). For a color version of this figure, see www.iste.co.uk/mazars/damage.zip*

### 1.3.2.2.1. Triaxial cell: hydrostatic test and axisymmetric triaxial test

With a high-performance triaxial cell, it is possible to perform a test such as ($\sigma_1 = \sigma_2 = \sigma_3$). Figure 1.15(c) shows an example of a response curve obtained presented in the coordinate system benchmark ($\sigma_m$, $\Delta V/V$). $\sigma_m$ is the hydrostatic

stress (or pressure) and $\Delta V/V = \varepsilon_1 + \varepsilon_2 + \varepsilon_3$ is the volume variation. The stress is normalized by the compressive strength.

The resulting behavior has three phases:

– a quasi-elastic phase; at the scale of the curve, it is small, but it makes it possible to show the bulk modulus:

$$K = \frac{(\sigma_1+\sigma_2+\sigma_3)}{3(\varepsilon_1+\varepsilon_2+\varepsilon_3)} = \frac{1}{3}\frac{E}{(1-2\vartheta)} \qquad [1.1]$$

– a phase of progressive collapse of the microporous matrix that generates a nonlinearity with increasing stress and a degradation of the medium that we will call consolidation (in the sense of soil mechanics), a mode very different from that related to the creation of a crack;

– a phase after collapse, gradually making the porosity filled with air disappear, it is then the compaction of the water, initially present in some pores, and that of the solid phase (grains + matrix). As a result, the behavior is very much influenced by the water content of the medium: the greater it is, the more prematurely the inflection of the curve upward occurs (Pontiroli et al. 2010).

In Figure 1.16, we show the results of a series of tests carried out with the triaxial cell of the Giga machine (3SR Grenoble, France), whose performance is unique in the world of concrete research (Gabet et al. 2008).

Figure 1.16(a) shows the scheme of the confinement system (possibly up to 1 GPa), the axial jack having a capacity of 10 MN. On a specimen with 70 mm diameter and 140 mm height, the possible axial pressures are of the order of 2.5 GPa. The concrete considered is ordinary concrete; its failure in uniaxial compression appears for $f_c$ = 34 MPa and a peak deformation of approximately 0.2%.

The principle of the test presented is as follows. Two loading phases are applied:

– a hydrostatic phase up to a given pressure value p (= $\sigma_m$);

– a phase with a constant lateral pressure $\sigma_2 = \sigma_3$ (= p) and axial charge $\sigma_x$ increasing until failure (see Figure 1.16(b)).

This was done for six values of p, from 0 (single compression) to p = 650 MPa. Figure 1.16(b) gives the corresponding loading paths in the coordinate system deviator ($\sigma_x$– p) average pressure (p); in the first phase, the deviator is zero, and in the second phase, it progresses at the same time as the axial load ($\sigma_x$) progresses.

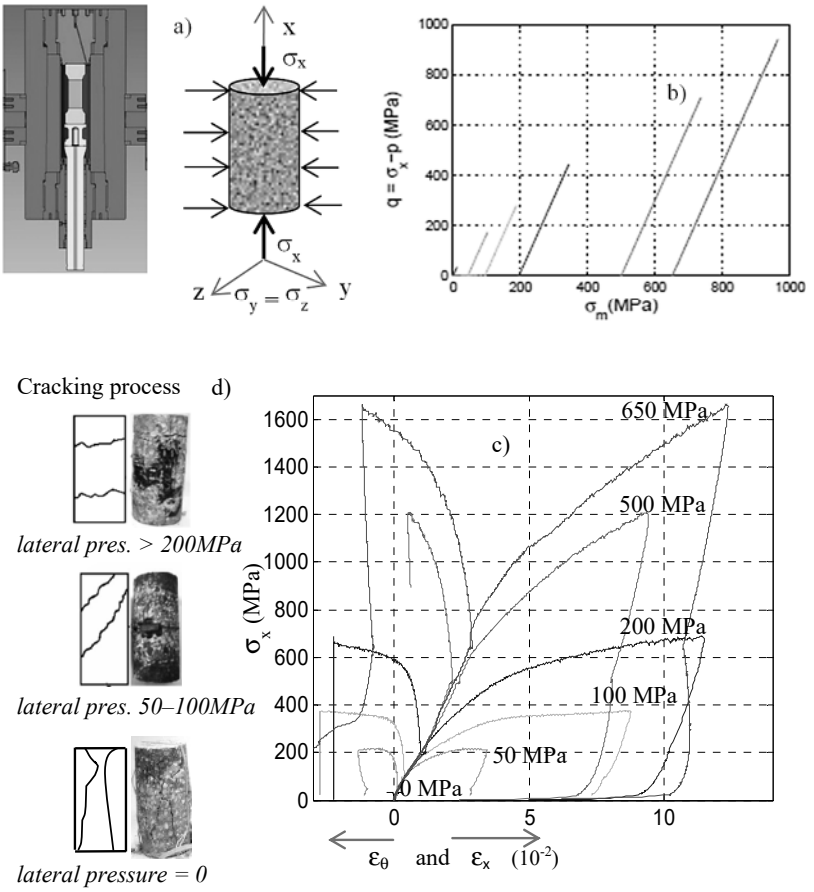


**Figure 1.16.** *Concrete response to triaxial loading. For a color version of this figure, see www.iste.co.uk/mazars/damage.zip*

COMMENTS ON FIGURE 1.16.– *(a) Scheme of the Giga confinement apparatus; (b) different loading paths: from a given hydrostatic pressure p, evolution of the deviator, $\sigma_x - p$, until failure (the lateral pressure $\sigma_y = \sigma_z$ being kept constant); (c) results for different values of the lateral pressure p from 0 to 650 MPa; (d) evolution of the crack facies from vertical in uniaxial compression to horizontal with a lateral stress greater than 200 MPa (from Gabet (2006)). $\varepsilon_\theta$ is the radial strain measured on the circumference of the specimen.*

The finding is that the value of the confinement pressure (p) has a major influence on the behavior obtained. Beyond 100 MPa of confinement, axial strains ($\varepsilon_x$) reach or exceed 10% and maximum stresses exceed 500 MPa.

These results show that confinement, by preventing any extension within the material and, consequently, any development of cracking in mode I, substantially increases the strength of concrete.

The analysis of the rupture is interesting. Figure 1.16(d) shows pictures of the crack facies obtained as a function of the intensity of the confinement. Starting from a globally vertical cracking for low confinements, we come to inclined cracks for medium confinements (50–200 MPa), which are the results of cracks in mode II (shear).

In this mode, due to confinement, the movements between the lips of cracks generate intense friction, and the energy to be spent to make them progress increases with p, giving the material a form of "ductility" (quasi-plateau with large strains).

Beyond a confinement to 200 MPa, we return to the observations made in the case of the hydrostatic test. The average stress $\sigma_m$ reaches values that intensely activate the consolidation; bands where this consolidation is located are then created inside the specimen in the weakest areas and perpendicular to the strongest stress ($\varepsilon_x$).

Additionally, noteworthy in these phases of failure is the incursion of the transverse (or radial $\varepsilon_\theta$) strain in the field of extensions, which favors the failure of the sample.

It is conceivable that, under these conditions, the modeling of such behaviors will have to include a number of specificities related in particular to degradation modes (mode I, mode II, consolidation) in relation to the possibilities or not of extensions and the existence of strong average stresses. Chapter 2 shows how these problems can be approached.

| Loading type | | Local damage mode | Behavioral peculiarities |
|---|---|---|---|
| **A** | – Uniaxial<br>– Biaxial<br>– Triaxial, with tension or low compression in at least one direction | Microcracking, first around the grains and then in the matrix, mainly in mode I; orthogonal cracks to the directions of extensions  | Existence of extensions in at least one direction. Behavior with peak and post-peak, modest strain value at failure (approximately $10^{-4}$ to $10^{-3}$) |

| | | | |
|---|---|---|---|
| **B** | Triaxial, superimposing hydrostatic pressure on a deviatoric pressure | Microcracking mainly in mode II with some confinement 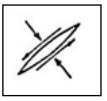 | Extension not allowed in all three directions. Ductile behaviour with significatant strain at failure (approximately $10^{-2}$) |
| **C** | Hydrostatic pressure creating a strong confinement | Collapse of microporosity generating consolidation 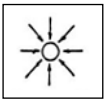 | Several phases of behavior: softening first then stiffening when the liquid (water) and solid (matrix + grains) phases are under pressure |
| **C'** | Triaxial combining strong confinement and deviator | Combination of type B and C damage modes and, under strong deviator, appearance of compression band localization | Like type B, ductile tendency behavior with high strain |

**Table 1.2.** *Summary of the different modes of damage according to the type of load and associated behavioral characteristics*

SUMMARY.– *Based on all the observations made throughout section 1.3, Table 1.2 proposes a classification of behaviors into four classes according to the type of load applied to a representative volume of concrete. These classes form the basis of the hypotheses and choices formulated to establish the behavioral models proposed in Chapter 3.*